INTERNATIONAL JOURNAL FOR NUMERICAL METHODS IN ENGINEERING
Int. J. Numer. Meth. Engng 2002; **53**:797–824 (DOI: 10.1002/nme.312)

Use of the tangent derivative boundary integral equations for the efficient computation of stresses and error indicators

K. H. Muci-Küchler[1,*,†], J. C. Miranda-Valenzuela[2] and S. Soriano-Soriano[3]

[1] *University of Detroit Mercy, Detroit, Michigan 48219-0900, U.S.A.*
[2] *ITESM Campus Toluca, San Antonio, Buenevista, Edomex 50110, Mexico*
[3] *Prolec GE, Power Division, Apodaca, NL 66600, Mexico*

SUMMARY

In this work, a new global reanalysis technique for the efficient computation of stresses and error indicators in two-dimensional elastostatic problems is presented. In the context of the boundary element method, the global reanalysis technique can be viewed as a post-processing activity that is carried out once an analysis using Lagrangian elements has been performed. To do the reanalysis, the functional representation for the displacements is changed from Lagrangian to Hermite, introducing the nodal values of the tangential derivatives of those quantities as additional degrees of freedom. Next, assuming that the nodal values of the displacements and the tractions remain practically unchanged from the ones obtained in the analysis using Lagrangian elements, the tangent derivative boundary integral equations are collocated at each functional node in order to determine the additional degrees of freedom that were introduced. Under this scheme, a second system of equations is generated and, once it is solved, the nodal values of the tangential derivatives of the displacements are obtained. This approach gives more accurate results for the stresses at the nodes since it avoids the need to differentiate the shape functions in order to obtain the normal strain in the tangential direction. When compared with the use of Hermite elements, the global reanalysis technique has the attraction that the user does not have to give as input data the additional information required by this type of elements. Another important feature of the proposed approach is that an efficient error indicator for the values of the stresses can also be obtained comparing the values for the stresses obtained through the use of Lagrangian elements and the global reanalysis technique. Copyright © 2001 John Wiley & Sons, Ltd.

KEY WORDS: adaptive meshing; Hermite boundary elements; hypersingular boundary integral equations; global reanalysis

1. INTRODUCTION

Nowadays, most of the analyses that are carried out using the boundary element method (BEM) are performed using Lagrangian elements for the functional representation of the field

*Correspondence to: K. H. Muci-Küchler, Department of Mechanical Engineering, University of Detroit Mercy, 4001 W. McNichols Road, P.O. Box 19900, Detroit, MI 48219-0900, U.S.A.
†E-mail: mucikh@udmercy.edu

Received 20 May 2000
Revised 12 September 2000

variables. In addition, the boundary integral equations (BIEs) that are commonly employed for the solution of elastostatic problems only involve the boundary values of the displacements and the tractions. Thus, when Lagrangian elements are used in conjunction with those BIEs, the stresses on the boundary are not immediately obtained once the system of equations generated by the BEM has been solved. Therefore, additional computations must be carried out in a post-processing fashion in order to determine the value of those stresses. The approach that is commonly employed for that purpose uses Hooke's law together with the tractions and the tangential derivatives of the displacements [1]. Since it is necessary to differentiate the functional representation for the displacements to obtain the tangential derivatives of those quantities, in general the numerical solution for the stresses will be less accurate than the one for the displacements and the tractions. Furthermore, in general the stresses will not be continuous across element boundaries because Lagrangian elements can only provide C^0 continuity for the displacements at those locations.

Several alternatives have been proposed to overcome the difficulties mentioned above. One approach is the use of BIEs in terms of tangential derivatives of the displacements. Gosh *et al.* [2] recast the conventional boundary integral equations (CBIEs) in terms of the tractions and the tangential derivatives of the displacements. This scheme provides satisfactory results but no longer involves the displacement function itself, which presents some uniqueness difficulties, especially on multiple connected regions.

In 1986, Watson [3] proposed the use of Hermitian interpolation functions to approximate the values of the displacements and the tractions inside an element. Since Hermite elements provide C^1 continuity for the displacements across element boundaries, the stresses will be continuous at those locations. Although in general Hermite elements provide very accurate results, this type of elements did not attract much attention from researchers and analysts in the BEM community. One of the main reasons was the difficulties that were initially encountered in the numerical implementation of the hypersingular equations used in their formulation. To tackle this problem, Muci-Küchler and Rudolphi [4] proposed completely regularized forms of the hypersingular boundary integral equations (HBIEs) to make their implementation easier and more robust. In addition, they implemented the Hermite elements in a non-isoparametric fashion, making their use more attractive.

However, Hermite elements still have the disadvantage that the user has to give the tangential derivatives of the quantities imposed as boundary conditions as input data, information that in some cases may not be readily available at first hand. Also, the functional representation used for the tractions involves the tangential derivatives of those quantities which do not necessarily have a relevant application in a practical context.

Another approach that could be used would employ the ideas presented by Gray and San Soucie [5]. In this case, the functional representation for the displacements is the same as the one employed for Hermite elements. However, the functional representation for the tractions corresponds to the one used for the Lagrangian elements. Under these circumstances, the nodal values of the tangential derivatives of the displacements can be considered as additional unknowns, and HBIEs are used to generate the additional equations required to obtain a solution.

Matsumoto, Tanaka and Hirata [6] presented another approach for the computation of the stresses based on performing two consecutive analyses. The first analysis solves for the displacements and the tractions using the CBIEs. For the second analysis, the components of the gradient of the displacement vector are approximated inside an element using the nodal values of those quantities and Lagrangian shape functions. To solve for the new unknowns,

regularized BIEs for displacement gradients are employed. This second analysis avoids the need to differentiate the functional representation for the displacements to compute the tangential derivatives of these quantities at any point on the boundary. Although this approach provides better results for the stresses, its high cost may makes it unattractive, especially for large models.

More recently, Chati and Mukherjee [7] presented an iterative scheme that makes use of regularized HBIEs in order to compute the stresses at regular points on the boundary at which the stresses are continuous. The authors applied the method to two different linear elasticity problems and in both cases reported successful results.

Two other approaches that do not employ equations in terms of derivatives of displacements are the use of spline elements and the use of additional high-order shape functions. The use of spline elements [8] gives continuity in the variable's derivatives by means of using continuous shape functions across elements. One disadvantage of this proposal is that "control points" outside the elements may be needed. In another approach, Zhao [9] enriches the elements using a high-order shape function to ensure continuity of the stress and stress gradient across elements. This scheme seems easy to implement but poses some problems when applied over non-smooth boundaries.

Independent of the type of formulation and elements employed, one way to increase the quality of the numerical solution obtained with the BEM is to selectively improve the discretization of the boundary using adaptive meshing techniques. In recent years, the number of references regarding adaptive meshing techniques in the BEM has increased significantly, and most of them are dedicated to formulate new and more reliable error indicators. In References [10, 11], a comprehensive list of contributions up to 1994 is provided. Since then, other alternatives have appeared. A brief explanation of some of the most relevant ones is presented in what follows.

Charafi *et al.* [12] used the local reanalysis technique to implement an efficient *h*-hierarchical adaptive meshing technique. They used a local enrichment scheme to obtain an improved solution for each element of the mesh. The improved solution was compared with the original one to obtain a measure of the error in the element.

Guiggiani [13] uses the direct differentiation approach to perform sensitivity analysis of approximate boundary element solutions with respect to the position of the collocation points. In a similar approach, Paulino *et al.* [14], use the rate of change of the tractions and generalized displacements with respect to the positions of middle nodes of quadratic boundary elements as error indicators. These rates of change are calculated by direct analytic differentiation of the governing equations for the type of problem under consideration. Gallego *et al.* [15] extend the work of Guiggiani [13] presenting sensitivity analysis of the solutions for the HBIE in the potential problem. In order to obtain the sensitivity equations, the derivative with respect to the position of the collocation point of the HBIE, is evaluated.

In Reference [16], Paulino *et al.* propose the evaluation of the residual of HBIEs as an error indicator. This methodology is developed for the approximation of the error on the boundary as well as in the interior of the domain. Liang *et al.* [17], use a modified version of the error indicator proposed by Paulino *et al.* combining the residuals of the CBIEs and HBIEs for the computation of error indicators. Menon *et al.* [18] present a basic iteration scheme that consists of using the BIEs for solving the boundary value problem and iterating this solution with the HBIEs. A residual is defined as the difference in the derivative quantities, and this residual is used as a BEM error estimate.

Muci-Küchler *et al.* [19], Muci-Küchler and Miranda-Valenzuela [20], and Miranda-Valenzuela *et al.* [21] presented formulations for the computation of simple error indicators for Hermite elements in potential, elastostatic, and thermoelastostatic problems in two dimensions. These error indicators were based on the possibility of obtaining two different numerical solutions for the tangential derivatives of the field variables from just one analysis with Hermite elements. The comparison of the two solutions inside an element was used as a measure of the error for that element.

Formulations that can recover better values for the stresses and at the same time lead to the obtention of reliable error indicators have been widely appreciated, especially in the finite element method. The superconvergent patch recovery technique developed by Zienkiewicz and Zhu [22, 23] and more recently, works like the one by Tessler *et al.* [24] follow this spirit, providing formulations that enable the recovery of more accurate stresses and the implementation of efficient error estimation and adaptive meshing techniques. Although the BEM is well suited to solve elastostatic problems, it seems that, nevertheless, a lack of such type of formulations exists.

In this work, a new global reanalysis technique, which uses the tangent derivative boundary integral equations (TDBIEs) for the efficient computation of stresses and error indicators in two-dimensional elastostatic problems is presented. The global reanalysis technique proposed here can be viewed as a post-processing activity that uses as a starting point the results provided by an analysis carried out employing Lagrangian elements. To perform the reanalysis, the functional representation for the displacements is changed from Lagrangian to Hermite, introducing the nodal values of the tangential derivatives of those quantities as additional degrees of freedom. Then, assuming that the nodal values of the displacements and the tractions remain practically unchanged from the ones obtained from the analysis using Lagrangian elements, the TDBIEs are collocated at each functional node in order to determine the new degrees of freedom that were introduced. In this fashion, a second system of equations is generated and, once it is solved, the nodal values of the tangential derivatives of the displacements are obtained. Hence, the nodal values of the stresses can be easily obtained and a more accurate functional representation for the displacements is available. Furthermore, an error indicator for each element can be computed by comparing the numerical solution for the stresses corresponding to the Lagrangian elements with the one computed using the results of the global reanalysis.

Finally, it is important to mention that it is very likely that the methodology proposed here can be extended for the solution of three-dimensional problems. Some of the necessary research work required in order to achieve that goal has already been published in the literature. Muci-Küchler and Rudolphi [25] have presented completely regularized versions of the TBIEs for three-dimensional elastostatic problems. Also, Muci-Küchler and Rudolphi have successfully formulated and implemented Hermite-like higher-order boundary elements for three-dimensional problems [26] and Muci-Küchler and Miranda-Valenzuela [27] have shown that it is possible to formulate a relaible and efficient error indicator for that type of elements.

2. BEM FORMULATION

In this section, a review of the boundary integral equations employed in this work is presented. Also, a briefing on how stresses are usually computed at a point on the boundary is given.

2.1. The conventional boundary integral equations

Consider the two-dimensional elastostatic problem without body forces. On a domain bounded by S, the CBIEs in a completely regularized form are given by [4]

$$\int_S T_{ij}(\mathbf{x},\boldsymbol{\xi})[u_j(\mathbf{x}) - u_j(\boldsymbol{\xi})]\,\mathrm{d}S(\mathbf{x}) = \int_S U_{ij}(\mathbf{x},\boldsymbol{\xi})t_j(\mathbf{x})\,\mathrm{d}S(\mathbf{x}) \tag{1}$$

where the range of indices goes from 1 to 2, and the summation convention is employed. Here, $\mathbf{x}$ represents the field point, $\boldsymbol{\xi}$ is the source point, and u_i and t_i are the displacement and traction components. The kernels U_{ij} and T_{ij} correspond to the standard fundamental solution for the elastostatic problem in two dimensions and are given by (see for example Reference [4]):

$$U_{ij}(\mathbf{x},\boldsymbol{\xi}) = \frac{-1}{8\pi\mu(1-\nu)}[(3-4\nu)\delta_{ij}\ln r - r_{,i}\,r_{,j}] \tag{2}$$

$$T_{ij}(\mathbf{x},\boldsymbol{\xi}) = \frac{-1}{4\pi(1-\nu)}\left(\frac{1}{r}\right)\left\{[(1-2\nu)\delta_{ij} + 2r_{,i}\,r_{,j}]\frac{\partial r}{\partial n} - (1-2\nu)(r_{,i}\,n_j - r_{,j}\,n_i)\right\} \tag{3}$$

In the above expression, where plain strain conditions have been considered, $r_{,i} = \partial r/\partial x_i = r_i/r$, r_i are the components of the position vector $\mathbf{r}$ that goes from $\boldsymbol{\xi}$ to $\mathbf{x}$, and n_i are the components of the unit outward normal vector at $\mathbf{x}$ (see Figure 1). In addition, μ is the shear modulus and ν the Poisson's ratio of the material that constitutes the domain.

2.2. The tangent derivative boundary integral equations

The tangent derivative equations are obtained by taking the derivatives of the displacement representation integral with respect to the source point coordinates ξ_i and taking the source point to the boundary. The resulting equations, in their completely regularized form, can be written as [4]

$$\begin{aligned}\int_S V_{ij}(\mathbf{x},\boldsymbol{\xi})\left[u_j(\mathbf{x}) - u_j(\boldsymbol{\xi}) - \frac{\partial u_j}{\partial\zeta}(\boldsymbol{\xi})r_m\zeta_m\right]\mathrm{d}S(\mathbf{x}) + \int_S Y_{ij}(\mathbf{x},\boldsymbol{\xi})\,\mathrm{d}S(\mathbf{x})\frac{\partial u_j}{\partial\zeta}(\boldsymbol{\xi})\\ = \int_S [W^o_{ij}(\mathbf{x},\boldsymbol{\xi})t_j(\mathbf{x}) - W_{ij}(\mathbf{x},\boldsymbol{\xi})t_j(\boldsymbol{\xi})]\,\mathrm{d}S(\mathbf{x})\end{aligned} \tag{4}$$

In the above expression, the kernels V_{ij}, Y_{ij}, W_{ij}, and W^o_{ij} for plain strain conditions are given by

$$V_{ij}(\mathbf{x},\boldsymbol{\xi}) = \zeta_k\frac{\partial T_{ij}}{\partial\xi_k} \tag{5}$$

$$Y_{ij}(\mathbf{x},\boldsymbol{\xi}) = \mu\left\{\frac{2\nu}{1-2\nu}\zeta_j(\zeta_k n_l - s_k v_l)\frac{\partial U_{il}}{\partial\xi_k} + \zeta_k n_l\zeta_l\frac{\partial U_{ij}}{\partial\xi_k} + \zeta_l(\zeta_k n_j - s_k v_j)\frac{\partial U_{il}}{\partial\xi_k}\right\} \tag{6}$$

$$W_{ij}(\mathbf{x},\boldsymbol{\xi}) = s_k\frac{\partial U_{ij}}{\partial\xi_k} \tag{7}$$

$$W^o_{ij}(\mathbf{x},\boldsymbol{\xi}) = \zeta_k\frac{\partial U_{ij}}{\partial\xi_k} \tag{8}$$

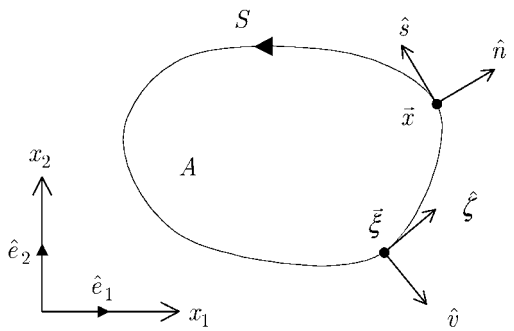

Figure 1. Problem domain, unit vectors, and global co-ordinate system.

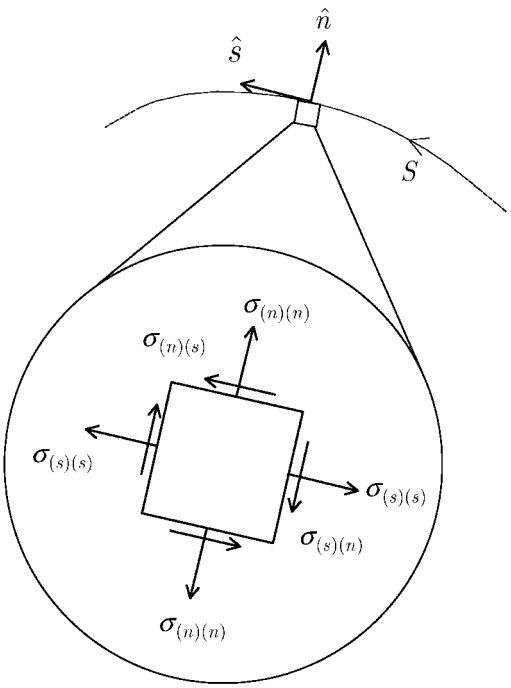

Figure 2. Components of the stress tensor in terms of a local co-ordinate system.

where s_k and n_k are the components of the unit tangent and normal vectors at $\mathbf{x}$, and ζ_k and v_k are the components of the unit tangent and normal vectors at $\boldsymbol{\xi}$ (see Figure 1). The kernel V_{ij} is $O(1/r^2)$ in the limit as $r \to 0$ while W_{ij} and W_{ij}^o are both $O(1/r)$ and Y_{ij} is $O(1)$, provided the boundary S has a continuous tangent at $\boldsymbol{\xi}$.

2.3. *Computation of the stresses*

Consider a model where an approximation for the displacements and tractions inside each element is available from the BEM solution. The first step in the computation of the stresses is the evaluation of the in-plane components of the stress tensor in terms of a local co-ordinate system (see Figure 2). For plane strain, the normal and shear stresses at a boundary point $\mathbf{x}$ can be obtained as

$$\begin{aligned}
\sigma_{(\mathrm{n})(\mathrm{n})} &= t_i n_i \\
\sigma_{(\mathrm{n})(\mathrm{s})} &= t_i s_i \\
\sigma_{(\mathrm{s})(\mathrm{s})} &= \frac{1}{1-\nu}[2\mu\varepsilon_{(\mathrm{s})(\mathrm{s})} + \nu\sigma_{(\mathrm{n})(\mathrm{n})}]
\end{aligned} \tag{9}$$

Although the normal stress $\sigma_{(\mathrm{n})(\mathrm{n})}$ and the shear stress $\sigma_{(\mathrm{n})(\mathrm{s})}$ are found in a straightforward fashion, the computation of the normal stress in the tangential direction $\sigma_{(\mathrm{s})(\mathrm{s})}$ requires the

prior computation of the normal strain in the tangential direction $\varepsilon_{(s)(s)}$ which is given by

$$\varepsilon_{(s)(s)} = \frac{\partial u_i}{\partial s} s_i \tag{10}$$

Here $\partial u_i/\partial s$ are the tangential derivatives of the displacement components. If the values of $\partial u_i/\partial s$ at the functional nodes are not directly available from the solution of the system of equations generated by the BEM, they have to be computed through the differentiation of the functional representation for the displacements employed inside the element. In the case of Lagrangian elements, which only offer C^0 inter-element continuity, this differentiation will lead in general to discontinuities in the values for the stresses across element boundaries. This, in general, will degrade the overall quality of the numerical solution for the stresses, specially across those element interfaces were the stresses are continuous.

3. THE GLOBAL REANALYSIS TECHNIQUE

The coincident collocation of the CBIEs and the TDBIEs to formulate Hermite boundary elements has proved to give very accurate results for the stresses [4, 26]. Even so, this type of elements has failed to attract the interest of researchers and users of the BEM. Researchers may feel discouraged due to the complexity involved in the implementation of Hermite elements in a computer code, and users may find that it is cumbersome for them to input more information than the one that is usually needed.

In this work, a new scheme that provides better results for the stresses than Lagrangian elements and avoids the necessity to provide additional information during the pre-processing stage is presented.

The global reanalysis technique proposed here can be viewed as a post-processing activity which uses as a starting point the results provided by an analysis carried out employing Lagrangian elements. To perform the reanalysis, the functional representation for the displacements is changed from Lagrangian to Hermite, introducing the nodal values of the tangential derivatives of those quantities as additional degrees of freedom.

Then, assuming that the nodal values of the displacements and the tractions remain practically unchanged from the ones obtained in the analysis using Lagrangian elements, the TDBIEs are collocated at each functional node in order to determine the new degrees of freedom that were introduced. In this fashion, a second system of equations is generated and, once it is solved, the nodal values of the tangential derivatives of the displacements are obtained.

3.1. First analysis

The first step towards the application of the global reanalysis technique is to perform an analysis using standard Lagrangian elements. This analysis is carried out without any particulars except from the fact that the subsequent application of the TDBIEs imposes some restrictions in the discretization of the boundary. These restrictions refrain from positioning functional nodes at corners and, for models in which subregions are employed, at points along the interfaces between subregions which are shared by more than two subregions or that also form part of the boundary of the domain. Hence, partially discontinuous or discontinuous elements should be selectively used to avoid the placement of functional nodes at those locations.

This first analysis solves for the nodal values of u_i and t_i through the use of the conventional boundary integral equations for the elastostatic problem in two dimensions

$$\int_S T_{ij}(\mathbf{x},\boldsymbol{\xi})[u_j(\mathbf{x}) - u_j(\boldsymbol{\xi})]\,\mathrm{d}S(\mathbf{x}) = \int_S U_{ij}(\mathbf{x},\boldsymbol{\xi})t_j(\mathbf{x})\,\mathrm{d}S(\mathbf{x}) \tag{11}$$

where the components of the displacement and traction vectors are interpolated using standard Lagrangian shape functions as follows:

$$u_i(\eta) = \sum_{K=1}^{NN} \hat{H}_K(\eta) u_i^{(K)} \tag{12}$$

$$t_i(\eta) = \sum_{K=1}^{NN} \hat{H}_K(\eta) t_i^{(K)} \tag{13}$$

In the above expressions η is the intrinsic or local co-ordinate in an element, NN is the total number of functional nodes in the element, and $\hat{H}_K$ is the Lagrangian shape function associated with the Kth functional node.

3.2. Second analysis

Once the values of the displacements and tractions are available at each functional node, the first step towards the second analysis is to change the functional representation for the displacements from Lagrangian to Hermite (see Figure 3).

After this change takes place, the functional representation for the displacements is enhanced due to the addition of the values of the tangential derivatives of these quantities at the functional nodes. Hence, the displacements will now be interpolated using Hermite shape functions [4]

$$u_i(\eta) = \sum_{K=1}^{NN} \left[H_K^{(1)}(\eta) u_i^{(K)} + H_K^{(2)}(\eta) \frac{\partial u_i^{(K)}}{\partial s} \right] \tag{14}$$

where $H_K^{(\alpha)}$ is the αth Hermite shape function associated with the Kth functional node.

It should be clear that only the functional representation for the displacements is changed, as the tractions would still be represented using Lagrangian shape functions. Also, it should be noted that the geometric representation of the element remains unchanged, if like in this work, the geometric description of the elements is dissociated from the functional representation of the boundary variables.

As of now, the second analysis involves the nodal values of the following field variables: u_i, t_i, and $\partial u_i/\partial s$. Making the assumption that the values for the displacement and tractions remain practically unchanged from the ones found in the first analysis, the values for those quantities can be taken from the first analysis instead of solving again for them. In this fashion, the only new unknowns added to the model are the nodal values of the tangential derivatives of the displacements $\partial u_i/\partial s$ (see Figure 4).

The unknown values of the tangential derivatives of the displacements at the functional nodes can be found by collocating the TDBIEs at each functional node in order to generate a new system of equations that solves for the nodal values of $\partial u_i/\partial s$. To generate the system of equations, it is useful to separate the integrals contained in the TDBIEs given by

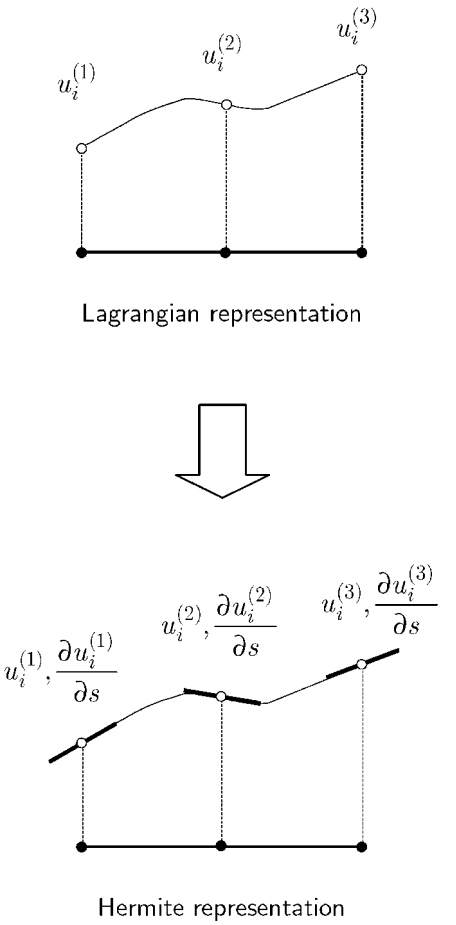

Figure 3. Change in the functional representation for the displacements from Lagrangian to Hermite.

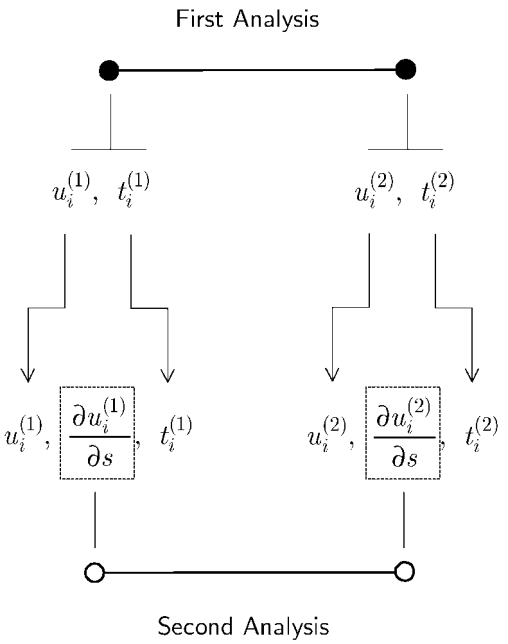

Figure 4. Field variables in the first and second analyses.

Equation (4) into several parts, depending on the type of singularity present in each one of the kernels and the part of the boundary over which the equations are being collocated.

Hence, Equation (4) can be now expressed as

$$\int_{S'} V_{ij}(\mathbf{x},\boldsymbol{\xi})u_j(\mathbf{x})\,\mathrm{d}S(\mathbf{x}) + \int_{S_o} V_{ij}(\mathbf{x},\boldsymbol{\xi})\left[u_j(\mathbf{x}) - u_j(\boldsymbol{\xi}) - \frac{\partial u_j}{\partial \zeta}(\boldsymbol{\xi})r_m\zeta_m\right]\mathrm{d}S(\mathbf{x})$$

$$- \int_{S'} V_{ij}(\mathbf{x},\boldsymbol{\xi})\,\mathrm{d}S(\mathbf{x})u_j(\boldsymbol{\xi}) + \int_{S} Y_{ij}(\mathbf{x},\boldsymbol{\xi})\,\mathrm{d}S(\mathbf{x})\frac{\partial u_j}{\partial \zeta}(\boldsymbol{\xi}) - \int_{S'} V_{ij}(\mathbf{x},\boldsymbol{\xi})r_m\zeta_m\,\mathrm{d}S(\mathbf{x})\frac{\partial u_j}{\partial \zeta}(\boldsymbol{\xi})$$

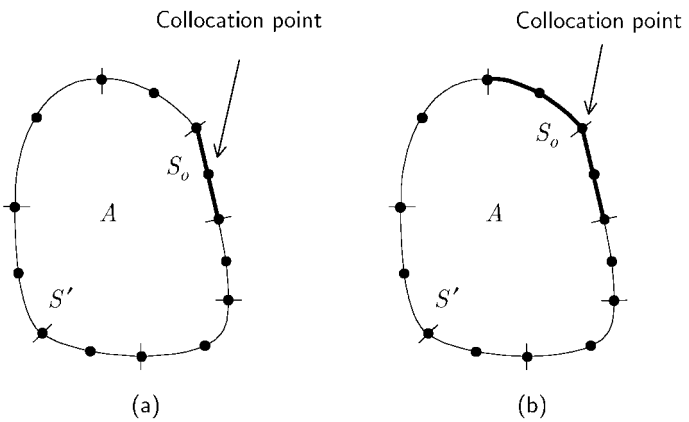

Figure 5. Division of the boundary into two parts for the implementation of the TDBIEs.

$$= \int_{S'} W_{ij}^{o}(\mathbf{x},\boldsymbol{\xi}) t_j(\mathbf{x})\, \mathrm{d}S(\mathbf{x}) + \int_{S_o} [W_{ij}^{o}(\mathbf{x},\boldsymbol{\xi}) t_j(\mathbf{x}) - W_{ij}(\mathbf{x},\boldsymbol{\xi}) t_j(\boldsymbol{\xi})]\, \mathrm{d}S(\mathbf{x}) - \int_{S'} W_{ij}(\mathbf{x},\boldsymbol{\xi})\, \mathrm{d}S(\mathbf{x}) t_j(\boldsymbol{\xi}) \tag{15}$$

where S_o is portion of the boundary which contains the collocation point (i.e., the element or pair of elements containing the source point), and S' is the rest of the boundary such that $S = S' + S_o$. Figure 5 shows how the boundary is divided into S' and S_o.

The collocation of the TDBIEs at each functional node will generate two equations per node, resulting initially in a system of equations which can be written in the following form:

$$\mathbf{V}\mathbf{u} = \mathbf{W}\mathbf{t} \tag{16}$$

where $\mathbf{V}$ and $\mathbf{W}$ are the coefficient matrices and $\mathbf{u}$ and $\mathbf{t}$ are column vectors.

At this point the matrix $\mathbf{V}$ contains contributions from the kernels V_{ij} and Y_{ij}, and $\mathbf{W}$ contains contributions from the kernels W_{ij}^{o} and W_{ij}. The vector $\mathbf{u}$ has the known values for u_i and the unknown values for $\partial u_i/\partial s$ at each functional node. Finally, the vector $\mathbf{t}$ is the vector containing the known values of t_i at each functional node.

Therefore, all the RHS of Equation (16) is known, and the coefficient matrix $\mathbf{V}$ can be condensed so that only the unknown values for $\partial u_i/\partial s$ appear on the column vector on the LHS. Hence, the system of linear equations given by Equation (16) can be reduced to

$$\mathbf{A}\mathbf{c} = \mathbf{z} \tag{17}$$

where $\mathbf{A}$ is a $2N \times 2N$ coefficient matrix, N being the total number of functional nodes in the model, and $\mathbf{c}$ is the column vector containing only the unknown nodal values for $\partial u_i/\partial s$.

It is important to mention that in the implementation of this work, the system $\mathbf{A}\mathbf{c} = \mathbf{z}$ is assembled directly, avoiding the need to construct the system $\mathbf{V}\mathbf{u} = \mathbf{W}\mathbf{t}$ first.

One advantage of the global reanalysis procedure proposed here is that there is no need to specify boundary conditions for $\partial u_i/\partial s$ as with Hermite elements, which simplifies the creation of the input data for the model to be solved. Also, since the global reanalysis technique can

Table I. Comparison of the approximate computational cost for different methods.

Method	System of equations First analysis	System of equations Second analysis	Approximate number of operations
Lagrangian	$2N \times 2N$	None	$8N^3$
Hermite	$4N \times 4N$	None	$64N^3$
Matsumoto *et al.*	$2N \times 2N$	$4N \times 4N$	$72N^3$
Global reanalysis	$2N \times 2N$	$2N \times 2N$	$16N^3$

be considered as a post-processing activity, its implementation into existing BEM codes is less cumbersome.

3.3. *Comparison of the computational cost*

It is interesting to present a comparison of the computational cost involved in the solution of the system(s) of equations generated by some of the different alternatives that make use of different sets of integral equations to determine the values of the stresses on the boundary. If Gaussian elimination is employed to solve a system of equations, the total number of operations required would be of the order of M^3, where M is the number of equations in the system. Table I shows the comparison between four different methods in terms of the total number of functional nodes present in the mesh, which is denoted by N. As can be seen from the table, for meshes with the same number of nodes, the methodology presented here requires less operations to solve the system(s) of equations than the Hermite elements and the method proposed by Matsumoto *et al.* [6].

4. COMPUTATION OF THE ERROR INDICATOR

One of the more traditional ideas for the formulation of error indicators is to use the difference between two numerical solutions with different number of degrees of freedom to obtain an approximate measure of the error in the most accurate of the two.

Suppose that for a given problem a sequence of approximate solutions for the boundary stresses $\hat{\sigma}_{ij}^{\{1\}}(\mathbf{x})$, $\hat{\sigma}_{ij}^{\{2\}}(\mathbf{x})$, $\hat{\sigma}_{ij}^{\{3\}}(\mathbf{x})$, etc. is available, and that each one of them has more degrees of freedom than the previous one. As the number of degrees of freedom increases, it is reasonable to expect that the resulting numerical solution will get closer to the exact solution if the method is converging to the latter. That is, if the sequence will converge to the exact solution as the number of degrees of freedom increases indefinitely then

$$\left|\sigma_{ij}(\mathbf{x}) - \hat{\sigma}_{ij}^{\{n\}}(\mathbf{x})\right| \to 0 \quad \text{as } n \to \infty \tag{18}$$

where $\sigma_{ij}(\mathbf{x})$ is the analytical solution, and $\hat{\sigma}_{ij}^{\{n\}}(\mathbf{x})$ has more degrees of freedom than $\hat{\sigma}_{ij}^{\{n-1\}}(\mathbf{x})$.

If this is the case, then two different approximate solutions in the sequence must approach arbitrarily close to each other, that is

$$\left|\hat{\sigma}_{ij}^{\{m\}}(\mathbf{x}) - \hat{\sigma}_{ij}^{\{n\}}(\mathbf{x})\right| \to 0 \quad \text{as } n, m \to \infty \tag{19}$$

since

$$\left|\sigma_{ij}(\mathbf{x}) - \hat{\sigma}_{ij}^{\{n\}}(\mathbf{x})\right| + \left|\sigma_{ij}(\mathbf{x}) - \hat{\sigma}_{ij}^{\{m\}}(\mathbf{x})\right| \geqslant \left|(\sigma_{ij}(\mathbf{x}) - \hat{\sigma}_{ij}^{\{n\}}(\mathbf{x})) - (\sigma_{ij}(\mathbf{x}) - \hat{\sigma}_{ij}^{\{m\}}(\mathbf{x}))\right|$$
$$= \left|\hat{\sigma}_{ij}^{\{m\}}(\mathbf{x}) - \hat{\sigma}_{ij}^{\{n\}}(\mathbf{x})\right| \tag{20}$$

The two approximate solutions with different number of degrees of freedom can be chosen almost arbitrarily as long as they fulfill the basic convergency requirements imposed by the numerical method. One convenient approach is to choose any first solution and choose as the second one, one with twice the number of degrees of freedom. This approach has been successfully used by Rencis and Mullen [28, 29], and more recently by Rodríguez and Power [30], both using Lagrangian elements to obtain both solutions. Another possible approach is to use Lagrangian elements to obtain the first solution, and then use Hermite elements to obtain the second one. For two-dimensional boundary elements having the same number of nodes, Hermite elements have twice the number of degrees of freedom per node than the Lagrangian ones, making the comparison possible.

The use of the difference between two approximate numerical solutions is a very effective way to obtain a measure of the error. Nevertheless, depending on the approached used, this technique may not be ideal to lead adaptive processes since it may involve a very high computational cost, especially if the second solution has twice the number of degrees of freedom than the original one. At some extent, some proposals exist to reduce this computational cost. One is the use of *h*-hierarchical functions [12]. Another approach is to consider that the desired values of the solution on all those elements whose computed error is below a certain prescribed value are the ones obtained from previous analyses [30].

For certain problems, or under some circumstances, it may be more useful to measure the error in the tangential derivatives of the field variables rather than in the field variables themselves. In those cases, Muci-Küchler *et al.* [19], and Muci-Küchler and Miranda-Valenzuela [20], demonstrated that the use of Hermite elements can eliminate the need of performing two BEM solutions at each step of the adaptive process. Since Hermite elements involve in their formulation the nodal values of the field variables and their tangential derivatives, it is possible to obtain two different numerical solutions for the tangential derivatives of the field variables from just one analysis with Hermite elements. The first solution is obtained through the use of the nodal values of the field variables and their tangential derivatives (which are obtained directly from the BEM solution) together with the derivatives of the Hermite shape functions. The second one is obtained through the use of the nodal values of the field variables and the differentiation of Lagrangian shape functions.

This procedure of comparing the two numerical solutions obtained from one analysis with Hermite element could be seen, in a sense, as an 'equivalent' of solving a model composed of Lagrangian elements, 'enriching' them to Hermite elements, and solving the new model. Then, the results for the tangential derivatives, or associated quantities, such as the boundary stresses, obtained from both models, are compared on an 'element by element' basis. An advantage of the approach used in References [19, 20] is that the absence of an analysis with Lagrangian elements makes the computation of the error indicator very fast.

The previous idea can be extended for its use with Lagrangian elements and the global reanalysis technique. The idea behind the computation of the error indicator is to try to estimate the error in the solution for the stresses using the difference between two numerical

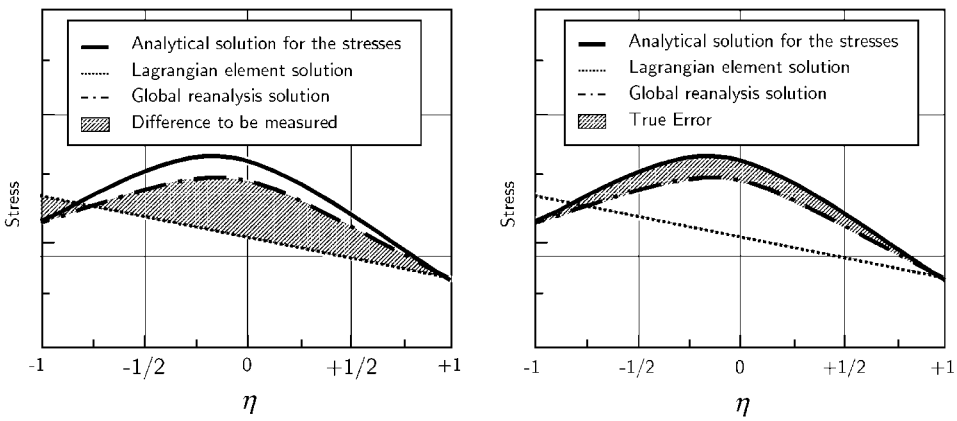

Figure 6. Comparison between the true error and the difference to be measured.

solutions for these quantities. In most cases, the difference between the global reanalysis results and the Lagrangian solution can be used as a reasonable upper bound of the magnitude of the error corresponding to the solution obtained using the global reanalysis technique. Figure 6 shows this idea graphically.

From Equations (9) and (10) it is clear that the computation of the boundary stresses in two dimensions depends on the following quantities: the normal and tangent unit vectors at the point of interest, the two components of the traction vector, and the tangential derivatives of the displacements. Since the normal and tangent unit vectors depend only on the geometry of the boundary, they will be the same for both solutions since they share the same geometric representation. The tractions will also be the same as their representation remains unchanged. On the other hand, in general, the values for the tangential derivatives of the displacements will be different since they require the use of the functional representation for the displacements.

The global reanalysis solution recovers directly the nodal values of $\partial u_i/\partial s$. If the value for the tangential derivatives of the displacements is needed at locations other than the functional nodes, they can be obtained through the differentiation of the Hermitian shape functions:

$$\frac{\partial u_i(\eta)}{\partial s} = \frac{1}{J(\eta)} \sum_{K=1}^{NN} \left(\frac{\partial H_1^{(K)}(\eta)}{\partial \eta} u_i^{(K)} + \frac{\partial H_2^{(K)}(\eta)}{\partial \eta} \frac{\partial u_i^{(K)}}{\partial s} \right) \tag{21}$$

where $J(\eta)$ is the reduced Jacobian of geometric transformation.

For the solution with Lagrangian elements, the values for the tangential derivatives of the displacements always have to be computed through the differentiation of the shape functions:

$$\frac{\partial u_i}{\partial s} = \frac{1}{J(\eta)} \sum_{K=1}^{NN} \left(\frac{\partial \hat{H}_K(\eta)}{\partial \eta} u_i^{(K)} \right) \tag{22}$$

The tractions are computed through their functional representation only if the point of interest does not correspond to a functional node:

$$t_i(\eta) = \sum_{K=1}^{NN} \left(\hat{H}_K(\eta) t_i^{(K)} \right) \tag{23}$$

Denoting the values for the stresses computed through Equation (21) as $\sigma^{(rg)}$ and the values for the stresses computed through Equation (22) as $\sigma^{(l)}$, the error indicator for the element can be computed measuring, in the L_2 norm, the difference between both quantities

$$\lambda_{\sigma}^{(e)} = \left\{ \int_{-1}^{1} \left[\sigma^{(rg)}(\eta) - \sigma^{(l)}(\eta)\right]^2 J(\eta)\, d\eta \right\}^{1/2} \tag{24}$$

Another way of measuring the difference between $\sigma^{(rg)}$ and $\sigma^{(l)}$ on an element is to compute the l_2 norm of the values of that difference at a discrete number of sample points distributed along the element. In this way, the error indicator is given by

$$\lambda_{\sigma}^{(e)} = \sqrt{\sum_{I=1}^{P} [\sigma^{(rg)}(\eta_I) - \sigma^{(l)}(\eta_I)]^2} \tag{25}$$

where P is the number of sample points selected, and η_I is the local co-ordinate associated with the Ith sample point.

The choice of using either summations or integrals to compute the error indicators is basically given in terms of computational cost. The use of integrals is usually more robust but involves a higher computational cost. The use of summations offers a very low computational cost, but some reliability in the computation of the error indicator may be compromised. For most analyses, the use of error indicators based on integrals computed using 6 or 8 Gaussian points seem to provide a good balance between reliability and cost. All the examples presented in this work were performed using this scheme. If the reader is interested in reviewing some results obtained through the summation approach, Muci-Küchler *et al.* [19], Muci-Küchler and Miranda-Valenzuela [20] and Miranda-Valenzuela *et al.* [21] present some examples for the potential, elastostatic, and thermoelastic problems in two dimensions, respectively.

Until now, nothing has been said about which specific stress component is considered in Equations (24) and (25). With the exception of $\sigma_{(n)(n)}$ and $\sigma_{(n)(s)}$, any stress component can be used to compute the error indicator inside each element. However, it must be mentioned that, in general, different stress components may lead to different adaptive meshing results. Also, it must be pointed out that the basic measure of the error is carried out in $\partial u_i/\partial s$. This opens the possibility for choosing a specific stress component if the analyst is particularly interested in the error in that specific component of the stress tensor. Furthermore, the user could measure the error in the von Mises stress, the maximum shear stress, or the maximum or minimum principal stress, as these stresses are commonly used for the design of mechanical components.

5. NUMERICAL EXAMPLES REGARDING STRESS ENHANCEMENT

Two sample problems are presented in order to show the advantages of the global reanalysis technique over the use of conventional Lagrangian elements alone for the computation of stresses. The first problem is one of an infinite plate with a circular hole subject to an uniaxial traction in the x_1 direction applied at infinity. The second problem corresponds to a thick wall cylinder subject to an internal pressure. Both problems are considered good choices since an analytical solution for each one is readily available [31] and the problems have moderate stress gradients.

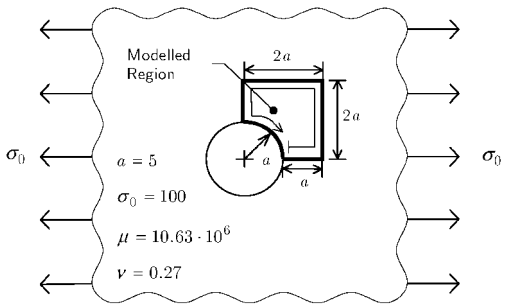

Figure 7. Boundary value problem for Example 1.

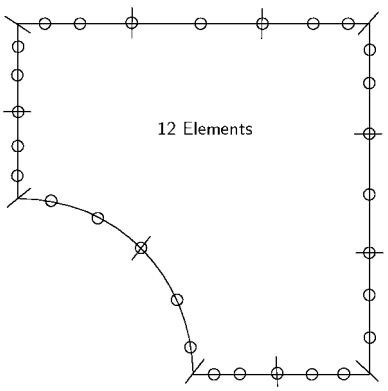

Figure 8. Proposed mesh for the comparison of results for Example 1.

5.1. Example 1: infinite plate with circular hole subject to an uni-axial traction

The boundary value problem for example 1 is presented in Figure 7. Owing to symmetry considerations, only one quarter of the problem was analyzed. In addition, a state of plain strain is assumed, and all the boundary conditions for the model are set to reflect the fact that only part of the infinite plate is being modelled. The model consisting of 12 quadratic Lagrangian elements shown in Figure 8 is adequate to demonstrate the increase in the accuracy of the solution for the stresses that is obtained when the global reanalysis technique is employed. Although the global reanalysis technique can be applied to any Lagrangian element, the use of quadratic elements is motivated by the great popularity that these elements have among the users of the BEM. A similar mesh of 3-noded Hermite elements is also analyzed to compare the performance of the global reanalysis technique against this type of elements.

Figure 9 presents a comparison of the numerical solutions obtained for the stress σ_{22} along the boundary $x_1 = 0$. In Figure 9(a), the Lagrangian, Hermite, and global reanalysis solutions are compared against the analytical one. As can be observed, the application of the global reanalysis technique increases the accuracy of the values of the stresses. The decrease in the true error can be seen more clearly in Figure 9(b) which plots the absolute true error in σ_{22} along the same boundary. From both figures, it is clear that the performance offered by Hermite elements is still superior than the one offered by the global reanalysis technique.

It is important to point out that the results presented in Figure 9 also show that, in general, Lagrange elements will provide discontinuous values for the stresses at functional nodes shared by more than one element. This behaviour is to be expected since Lagrange elements can only provide C^0 continuity for the displacements across element interfaces and the computation of the stresses makes use of the tangential derivative of the displacements.

Similar plots are presented in Figure 10 for the stress σ_{11} along the boundary $x_2 = 0$. As in the previous plots, the application of the global reanalysis technique enhances the performance of the Lagrangian elements. Once more, the Hermite elements still have the best performance.

It is clear now that the global reanalysis technique significantly increases the accuracy of the Lagrangian elements. It is also clear that the Hermite elements are still superior to the global reanalysis technique in performance. However, the computational cost of using

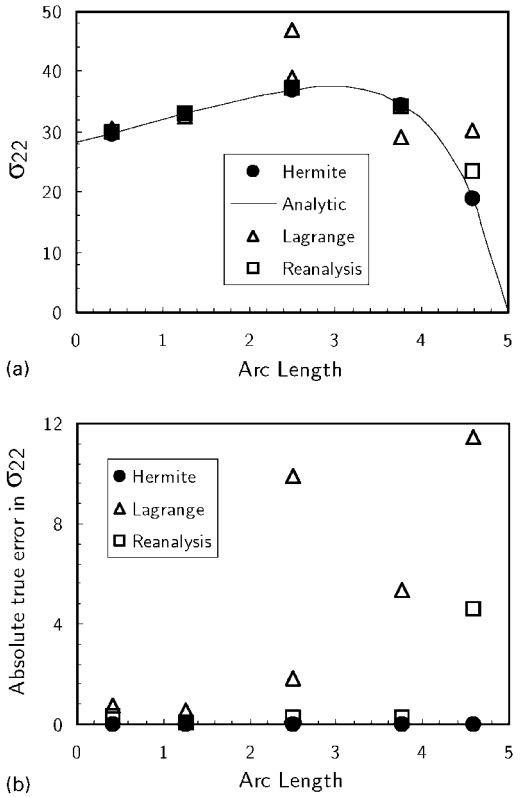

Figure 9. Comparison of the results for σ_{22} along the boundary $x_1 = 0$ for the different analyses using 3-noded elements: (a) against analytical solution; (b) absolute errors.

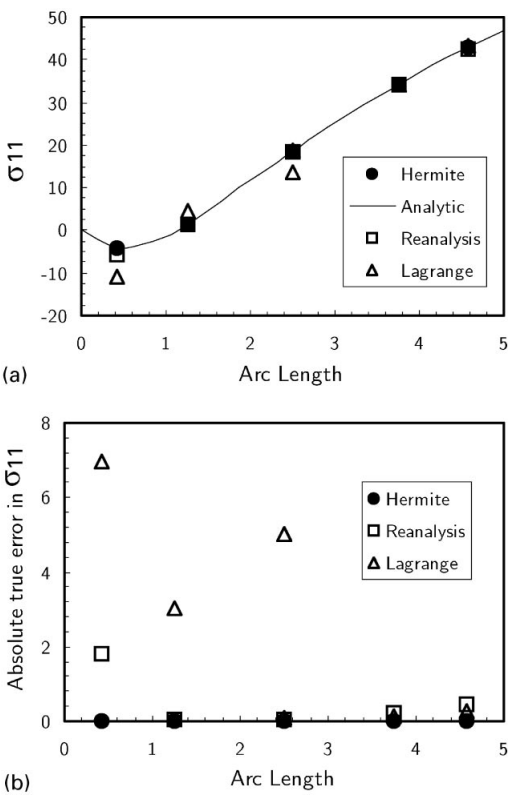

Figure 10. Comparison of the results for σ_{11} along the boundary $x_2 = 0$ for the different analyses using 3-noded elements: (a) against analytical solution; (b) absolute errors.

Hermite elements is higher than the one for the global reanalysis technique. In the same way, the global reanalysis technique has a higher computational cost than the use of Lagrangian elements alone. Now, the following question can be posed: Is the better performance of the Hermite elements and the global reanalysis technique just a result of their higher computational cost?

To clarify the previous point, and in order to do a fair evaluation of the quality of the solutions obtained with the global reanalysis technique and with the Hermite and Lagrangian elements, a comparison based on a similar number of floating point operations (flops) needed to solve the system(s) of equations is presented. For this purpose three different meshes are employed, one for the analysis with Lagrangian elements, one for the analysis with Hermite elements, and one for the analysis using the global reanalysis technique proposed in this paper. Using the formulas given in Table I, the solution of the system of equations generated by these three models involves a similar number of flops. Figure 11 presents the meshes used for the Lagrange, Hermite, and global reanalysis models. The figures show the approximate number of floating point operations required to solve the resultant system(s) of linear algebraic

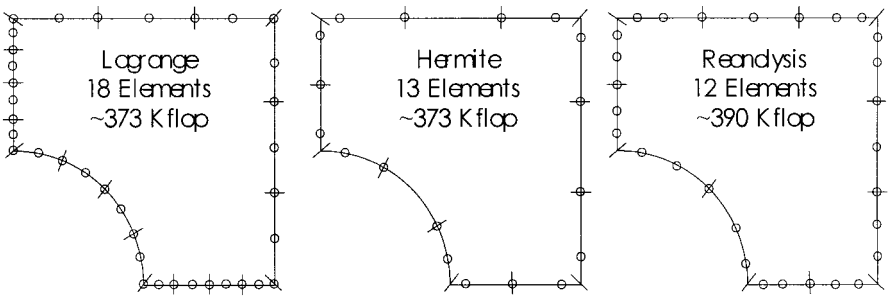

Figure 11. Different meshes used to compare the performance of the global reanalysis technique against Lagrangian and Hermite elements in Example 1 (only functional nodes are shown).

equations. It should be noted that the mesh for global reanalysis involves a slightly higher number of operations as a perfect match for the other two meshes can not be obtained. This additional cost is less than the cost associated with one node of the model.

Figure 12 shows the results for the stress σ_{22} along the boundary $x_1 = 0$ corresponding to the three different analyses. From these plots, it is clear that the application of the global reanalysis technique still has a positive impact on the accuracy of the solution. It is also evident in both plots that, for approximately the same computational cost, Hermite elements are still a better option in terms of performance.

In Figure 13 the results for stress σ_{11} along the boundary $x_2 = 0$ are shown. Similar to the results previously discussed, the application of the global reanalysis technique offers an advantage over the Lagrangian elements for the same computational cost. Once more, the plots also show the superior performance of the Hermite elements.

The previous plots offer an evidence of the better accuracy offered by Hermite elements. Despite this advantage, Hermite elements are not a popular choice among researchers and users of the BEM. One of the reasons is that their use is more involved as the user must specify the tangential derivatives of the boundary conditions as part of the input data. Hence, although the global reanalysis technique is inferior in performance to the use of Hermite elements, it is still a very appealing option as it combines the easiness of use of Lagrangian elements with a performance almost as high as the one of the Hermite elements.

5.2. Example 2: thick wall cylinder subject to an internal pressure

The boundary value problem for the second example is shown in Figure 14. This axisymmetric problem is modelled using one quarter of the original model. The cylinder is considered to be sufficiently long so that plain strain conditions prevail inside the continuum. For this example, the first mesh analyzed consisted of eight 3-noded elements, 2 per each boundary segment. In this simple axisymmetric problem, the interest will be focused on the von Mises stress distribution along the radial direction.

The behaviour of the Lagrangian, Hermite and global reanalysis solutions for the von Mises stress along the radial direction is shown in Figure 15. In Figure 15(a) the three solutions are compared with the analytical one, and in Figure 15(b) the absolute true errors for the solutions are compared. As with the previous example, the application of the global reanalysis technique gives an increased accuracy in comparison to the standard Lagrangian elements.

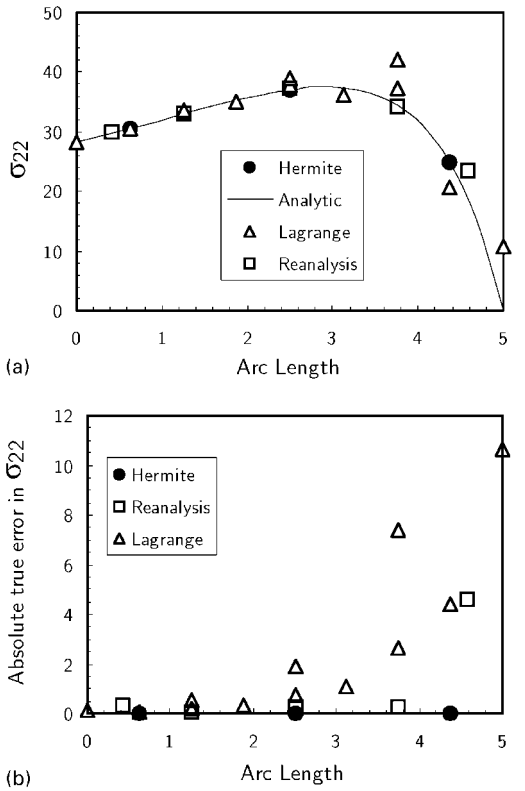

Figure 12. Comparison of results for σ_{22} along the boundary $x_1 = 0$ between the different analyses using a similar number of operations: (a) against analytical solution; (b) absolute errors.

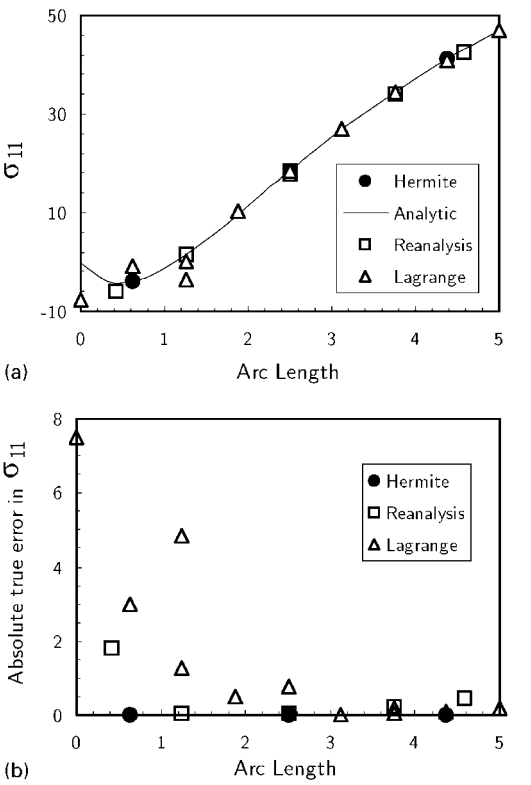

Figure 13. Comparison of results for σ_{11} along the boundary $x_2 = 0$ between the different analyses using a similar number of operations: (a) against analytical solution; (b) absolute errors.

The previous comparison was also carried out using a similar number of floating point operations. Figure 16 shows the meshes for the Lagrangian, Hermite, and global reanalysis models together with the approximate number of operations needed to solve the system of equations generated by each model.

Figure 17 shows the results for a similar number of operations. As can be seen in the figure, the global reanalysis technique improves the Lagrangian solution. In all the numerical experiments that have been carried out so far, the global reanalysis technique generally gives a better solution than the Lagrangian elements alone for a similar computational cost.

6. NUMERICAL EXAMPLES REGARDING ADAPTIVE MESHING

To test the error indicator based on stresses, four different problems from linear elasticity were selected. The first two problems, an infinite plate with a circular hole subject to an uni-axial tension, and a cylinder subject to an internal pressure, are the same ones that were considered

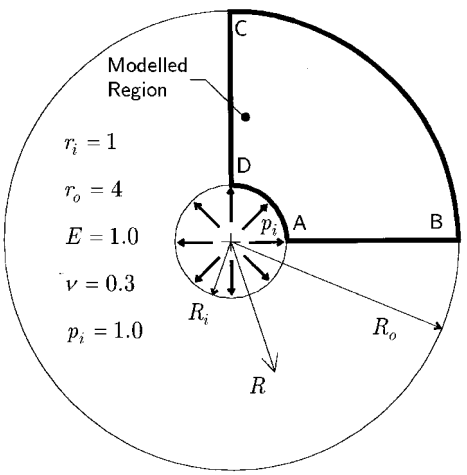

Figure 14. Boundary value problem for Example 2.

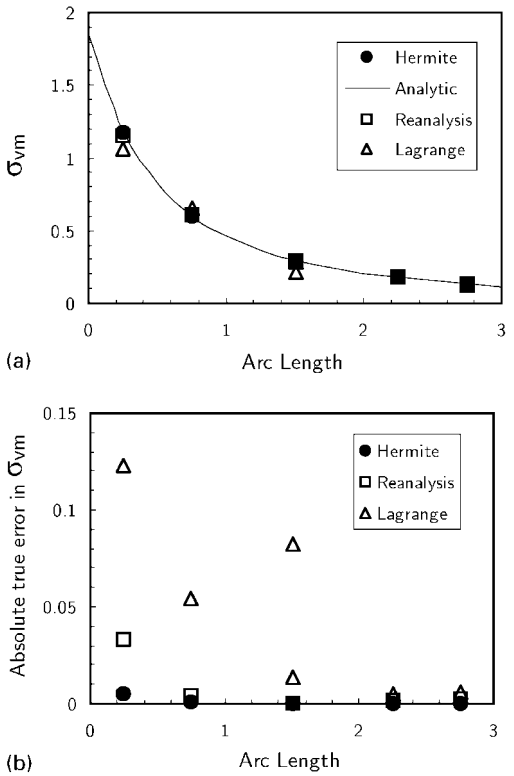

Figure 15. Comparison of results for the von Mises stress along the radial direction for the different analyses using 3-noded elements: (a) against analytical solution. (b) absolute errors.

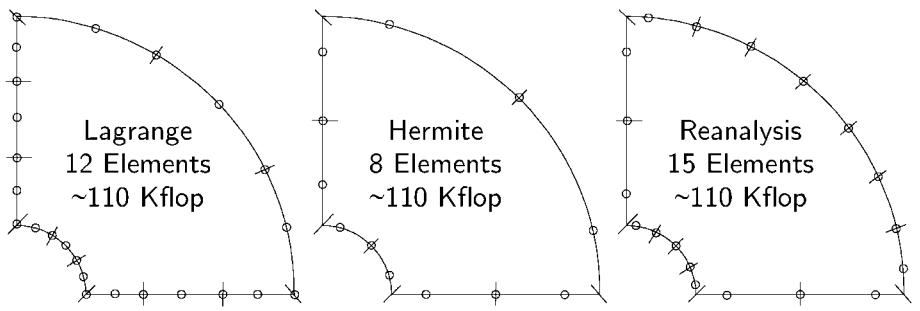

Figure 16. Different meshes used to compare the performance of the global reanalysis technique against Lagrangian and Hermite elements in Example 2 (only functional nodes are shown).

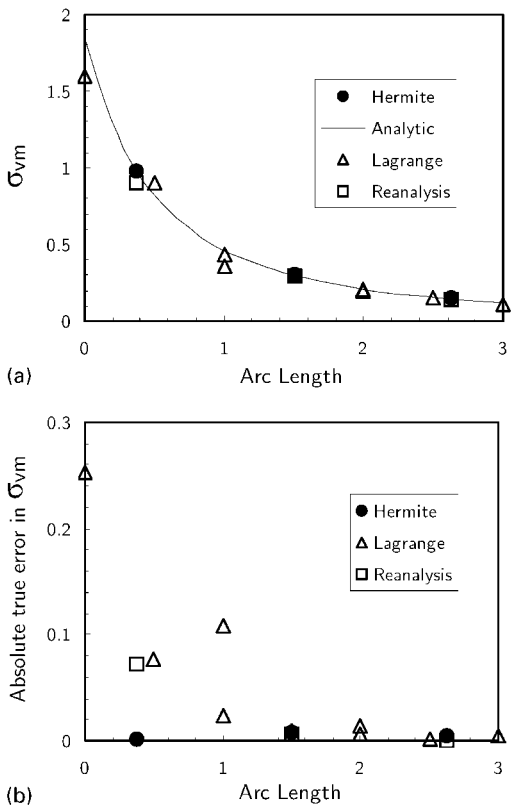

Figure 17. Comparison of results for the von Mises stress along the radial direction for the different analyses using a similar number of operations: (a) against analytical solution; (b) absolute errors.

in the previous section. The other two, a L-shaped domain subject to an uni-axial traction, and a stress concentration problem of complex geometry, have been used as benchmark problems by different authors.

To show how the error indicator works for design problems, the von Mises stress was selected as the stress used to lead the adaptive process in all examples.

6.1. Example 1: infinite plate with a circular hole under uni-axial tension

The first example is an infinite plate with a circular hole subject to a uniaxial traction in the x_1 direction as shown in Figure 7. This problem has been used extensively as a benchmark problem for adaptive meshing implementations. Several authors have presented it, including Guiggiani [32], Charafi, Neves and Wrobel [12], and Chao and Lee [33], among others.

The initial mesh for the adaptive analysis consisted of 12 quadratic elements. The refinement criteria consisted in refining into two elements of equal size all those elements whose value for the error indicator was larger than 2 (2 per cent of the applied load). For this analysis, the stop criterion was to request that all the elements of the final mesh should have a predicted error of less than 2.

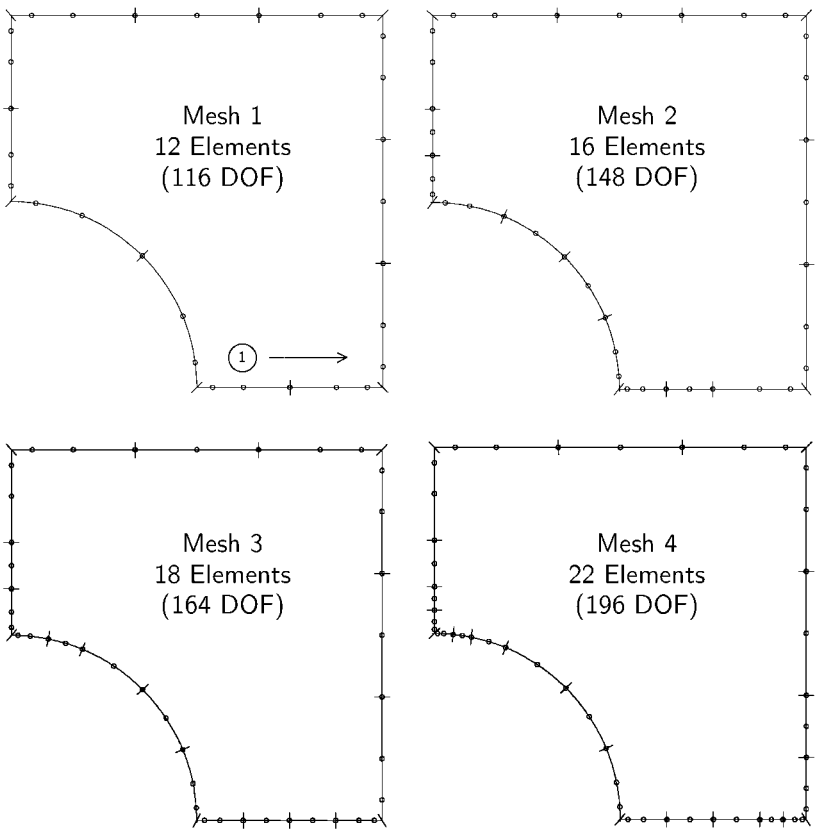

Figure 18. Meshes for the adaptive process of Example 1.

The adaptive process took 4 iterations to complete. Figure 18 shows the meshes corresponding to the adaptive process. In the figure, the number of degrees of freedom specified for each mesh includes the degrees of freedom added by the global reanalysis.

It is important to mention that although the new elements had half the size of the original ones, they did not necessarily have the same functional type if they were partially discontinuous or discontinuous. For example, a discontinuous element leads to one element partially discontinuous by the left, and one partially discontinuous by the right. In the same fashion, a partially discontinuous element by the right leads to a continuous element by the left, and a partially discontinuous element by the right, and so on. Also, it has to be mentioned that the ratio of the lengths between two adjacent elements were kept in the range from 0.25 to 4.0 to avoid possible errors in the numerical integration. This condition is known as the *compatibility condition for integration* and was proposed by Guiggiani [32].

As can be observed from the last mesh, the error indicator leads to a refinement of the elements located in the part of the boundary corresponding to the circular hole as well as the parts of the boundary adjacent to it, i.e. the bottom and left edges of the modelled region. This refinement agrees with the one presented by other authors for the same problem [32, 12].

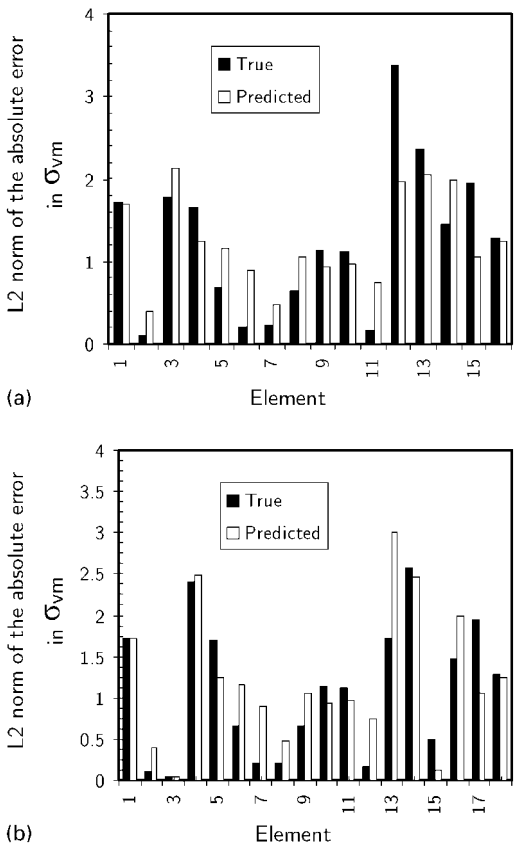

Figure 19. Comparison between the predicted and true errors in the von Mises stress for the adaptive process of Example 1: (a) second mesh; (b) third mesh.

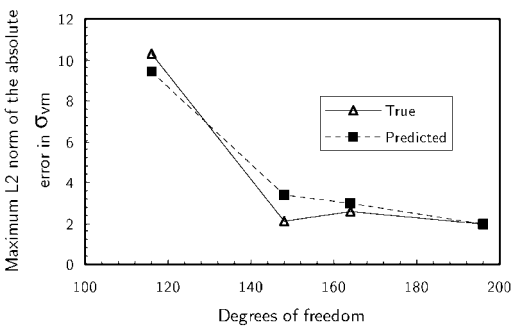

Figure 20. Convergence to the analytical solution in the adaptive process of Example 1.

A comparison between the true and predicted errors for the elements in the second and third meshes is presented in Figure 19. Both plots show a good agreement between the predicted and true errors for all the elements in the model. This agreement is also reflected in Figure 20 where the behaviour of the maximum value for the true and predicted errors at each step of the adaptive process is presented.

6.2. Example 2: cylinder under internal pressure

The second problem is a thick wall cylinder subject to an internal pressure as shown in Figure 14. The analytical solution for the von Mises stress in this problem is constant along the internal and external circular boundaries and varies from its minimum value at the outer radius to its maximum value at the inner radius. Therefore, it is reasonable to expect fewer element along the curved boundaries and more elements along the line segments AB and CD, concentrated towards the points which have the highest value for the stress, namely, points A

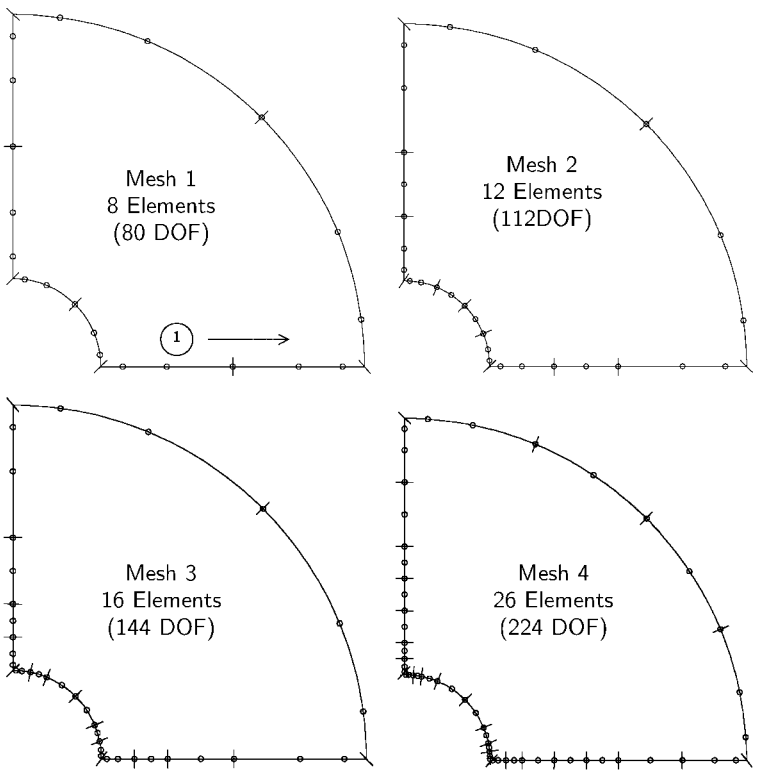

Figure 21. Meshes for the adaptive process of Example 2.

and D. Furthermore, the refinement along the line segments AB and CD must be symmetrical due to the nature of the problem.

The starting point for the adaptive process was an initial mesh with 8 quadratic Lagrangian element distributed evenly along the boundary. In this case, all the elements with a predicted error larger than the average value for the same quantity were refined in two elements of equal size. The adaptive process was stopped after 4 iterations.

Figure 21 shows the meshes corresponding to the adaptive process where the number of degrees of freedom for each mesh reflects the additional degrees of freedom included by the global reanalysis. The final mesh agrees with the behavior of the analytical solution, but presents some refinement on the internal boundary near points A and D. This refinement is due to small variations in the approximation of the circular geometry which causes gradients in the numerical solution for the stresses in an otherwise constant solution. This gradients are sufficient enough to make the error indicator report an error that is above the average value. Other authors like Paulino *et al.* [14] report similar final meshes showing a mesh refinement in the internal boundary.

Figure 22 shows a comparison between the predicted and true errors for the elements of the first and second meshes. The plots show a good agreement between the true and the predicted errors, although some over- and under-prediction of the error in the elements near

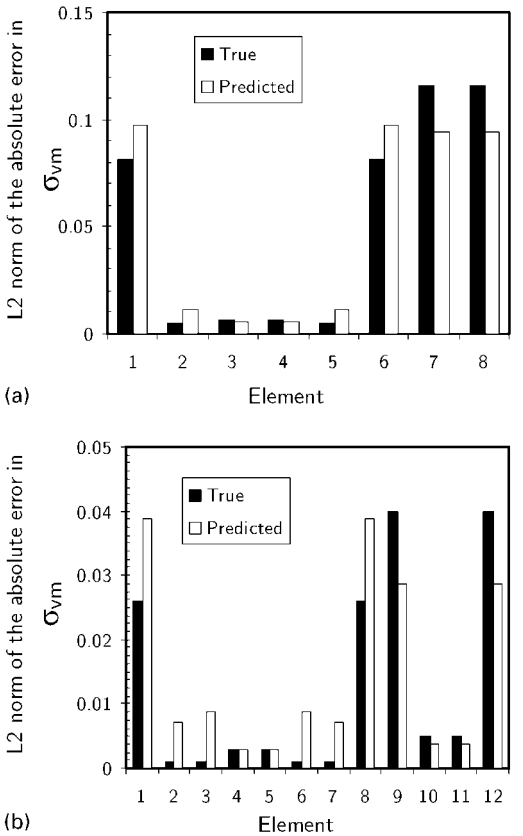

Figure 22. Comparison between the predicted and true errors in the von Mises stress for the adaptive process of Example 2: (a) first mesh; (b) second mesh.

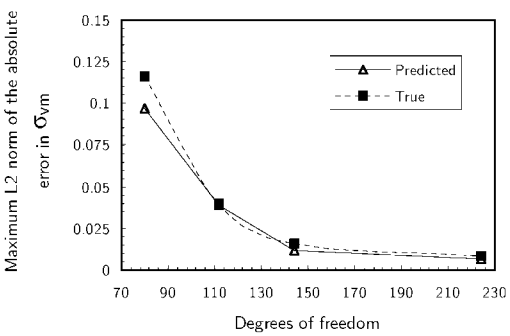

Figure 23. Convergence to the analytical solution in the adaptive process of Example 2.

points A, B, C and D is evident. This behaviour is likely to be related to the use of partially discontinuous elements.

The behaviour of the maximum absolute value for the predicted and true errors in the adaptive process is presented in Figure 23. As can be seen, the true and the predicted errors show a very good agreement and both tend to zero as the mesh is refined. In this plot the number of degrees of freedom for each analysis reflects the additional degrees of freedom included by the global reanalysis.

6.3. Example 3: L-shaped domain

As third example, the L-shaped domain shown in Figure 24 is considered. Plane strain conditions are assumed and a traction $t = 1$ is applied to the model as can be seen in the figure. Although the analytical solution for this problem is not available, it has been analyzed by other authors [12] which makes possible a comparison of results. The problem has a re-entrant corner which originates a singular behaviour in the stresses.

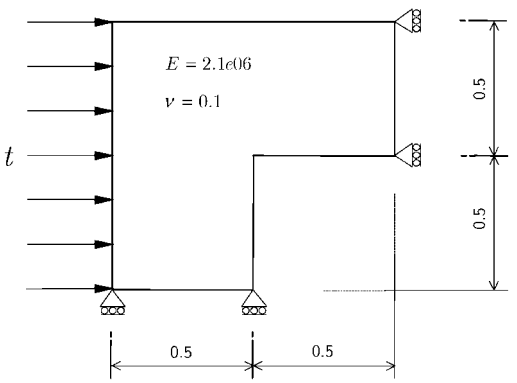

Figure 24. Boundary value problem for Example 3.

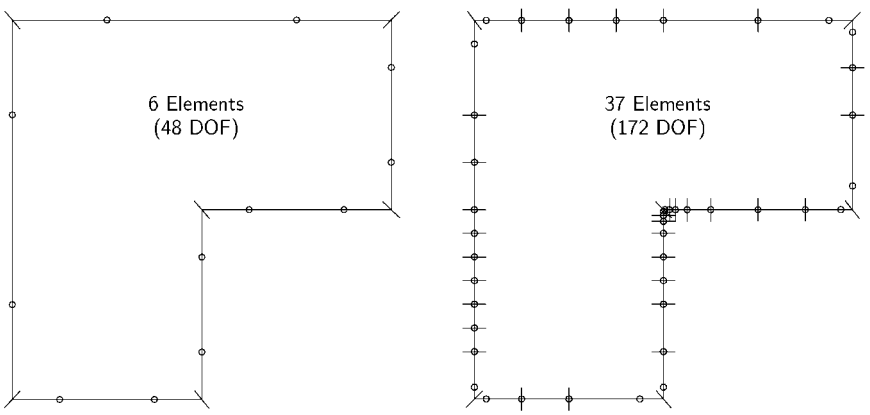

Figure 25. Initial and final meshes for the adaptive process of Example 3.

This problem was run using linear Lagrangian elements to show how the global reanalysis technique behaves with this type of element. In this adaptive process, all those elements with a value for the predicted error larger than 0.05 (5 per cent of the imposed load) were refined into two elements of equal size. The adaptive process was stopped after six iterations.

The initial and final meshes for the problem under consideration are shown in Figure 25. The final mesh has an element distribution which is very similar to that for the adaptive analysis presented by Charafi *et al.* [12]. As the problem presents a singularity in the form of a re-entrant corner, it was reasonable to expect that the refinement should concentrate in this area.

Figure 26 shows the behaviour of the maximum value for the predicted error at each step of the adaptive process. The last mesh reported a maximum value for the von Mises stress of 10.36. This value is in good agreement with a 'reference' value of 10.8393. This reference value was obtained with a uniform mesh of 96 quadratic Lagrangian elements (384 degrees of freedom).

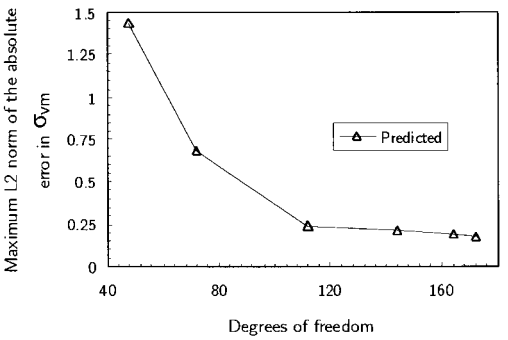

Figure 26. Behaviour of the maximum value for the predicted error in the adaptive process of Example 3.

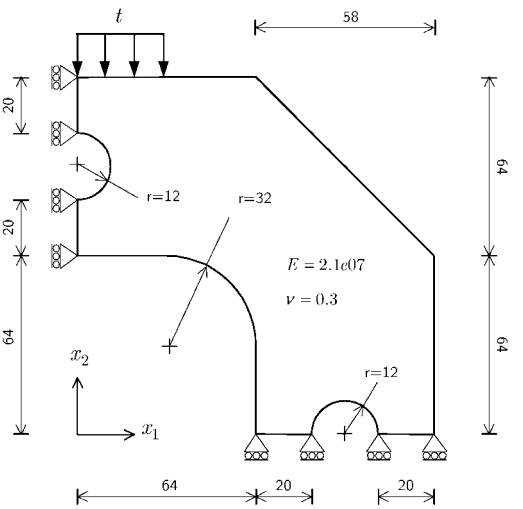

Figure 27. Boundary value problem for Example 4.

6.4. *Example 4: component with complex geometry*

The last example is a component with complex geometry. The boundary value problem for this example is presented in Figure 27 where the traction t is taken as 1. Owing to symmetry, only one quarter of the model is analyzed as shown. This example has been addressed by Guiggiani [32], and Charafi *et al.* [12].

For this example all the elements with a value for the predicted error larger than the average value for the same quantity were refined into two elements of equal size. The starting mesh had 15 quadratic Lagrangian elements. The adaptive process was stopped after five iterations.

The initial and final meshes for this problem are shown in Figure 28. This final mesh compares favourably with the meshes presented in References [12, 32].

Finally, Figure 29 presents the behaviour of the maximum value for the predicted error at each step of the adaptive process. The final mesh for this analysis reports a maximum value for the von Mises stress of 2.5408. This value is in very good agreement with a reference value of 2.5414 obtained using a mesh with 128 quadratic Lagrangian elements (512 degrees of freedom) distributed evenly along the boundary.

7. CONCLUSIONS

A new technique for the computation of stresses and error indicators in the Boundary Element Method has been presented. The global reanalysis technique uses the TDBIEs in a post-processing fashion to improve the solution for the stresses when an analysis with Lagrangian elements has already been performed. Its main attraction is that it increases the overall accuracy of the numerical solution for the stresses at a reasonable computational cost.

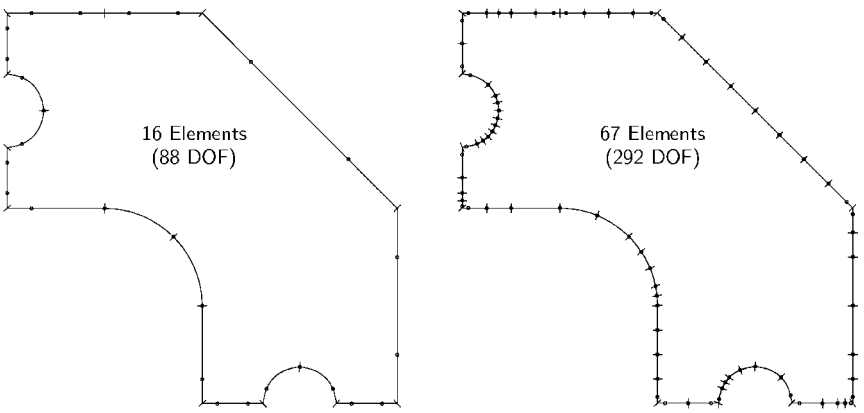

Figure 28. Initial and final meshes for the adaptive process of Example 4.

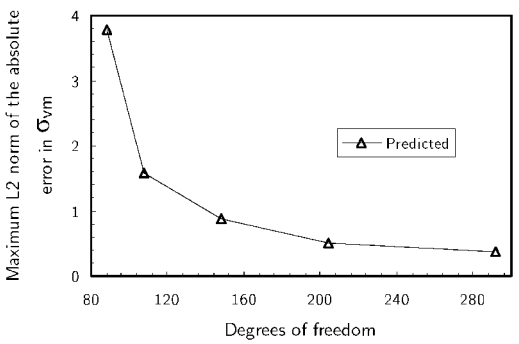

Figure 29. Behaviour of the maximum value for the predicted error in the adaptive process of Example 4.

Although the methodology is less accurate than the use of Hermite elements, it avoids the inconveniences of having to specify the tangential derivatives of the boundary conditions as part of the input data. The global reanalysis technique is also computationally cheaper than other proposals of the same type and can be implemented as a post-processing activity. In addition, an efficient and reliable error indicator capable of leading and adaptive meshing process can be computed from the difference between the original and the global reanalysis solutions, which adds another advantage to the proposed method.

REFERENCES

1. Becker AA. *The Boundary Element in Engineering—A Complete Course*. McGraw Hill International: New York, 1992.
2. Ghosh N, Rajiyah H, Ghosh S, Mukherjee S. A new boundary element method formulation for linear elasticity. *Journal of Applied Mechanics Transactions ASME* 1986; **53**:69–76.
3. Watson JO. Hermitian cubic and singular elements for plane strain. In *Developments in Boundary Element Methods-4*, Chapter 1. Banerjee PK, Watson JO (eds). Elsevier Applied Science Publishers: London, 1986.
4. Muci-Küchler KH, Rudolphi TJ. Coincident collocation of displacement and tangent derivative boundary integral equations in elasticity. *International Journal for Numerical Methods in Engineering* 1993; **36**:2837–2849.

5. Gray LJ, San Soucie CA. A Hermite interpolation algorithm for hypersingular boundary integrals. *International Journal for Numerical Methods in Engineering* 1993; **36**:2357–2367.
6. Matsumoto T, Tanaka M, Hirata H. Boundary stress calculation using regularized boundary integral equation for displacement gradients. *International Journal for Numerical Methods in Engineering* 1993; **36**:783–797.
7. Chati MK, Mukherjee S. Evaluation of gradients on the boundary using fully regularized hypersingular boundary integral equations. *Acta Mechanica* 1999; **135**:41–55.
8. Cabral JJS, Wrobel LC, Brebbia CA. A BEM formulation using B-splines: I-uniform blending functions. *Engineering Analysis* 1990; **7**:136–144.
9. Zhao Z. Interelement stress evaluation by boundary elements. *International Journal for Numerical Methods in Engineering* 1996; **39**:2399–2415.
10. Liapis S. A review of error estimation and adaptivity in the boundary element method. *Engineering Analysis* 1994; **14**:315–323.
11. Kita E, Kamiya N. Recent studies on adaptive boundary element methods. *Advances in Engineering Software* 1994; **19**:21–32.
12. Charafi A, Neves AC, Wrobel LC. *h*-Hierarchical adaptive boundary element method using local reanalysis. *International Journal for Numerical Methods in Engineering* 1995; **38**:2185–2207.
13. Guiggiani M. Sensitivity analysis for boundary element error estimation and mesh refinement. *International Journal for Numerical Methods in Engineering* 1996; **39**:2907–2920.
14. Paulino GH, Shi F, Mukherjee S, Ramesh P. Nodal sensitivities as error estimates in computational mechanics. *Acta Mechanica* 1997; **121**:191–213.
15. Gallego R, Martínez-Castro A, Suarez J. Sensitivity analysis of approximate solutions for the hypersingular boundary element method. In *Proceedings of the Boundary Elements Techniques Conference*, Aliabadi MH (ed.). London, 1999; 311–319.
16. Paulino GH, Gray LJ, Zarikian V. Hypersingular residuals—a new approach for error estimation in the boundary element method. *International Journal for Numerical Methods in Engineering* 1996; **39**:2005–2029.
17. Liang MT, Chen JT, Yang SS. Error estimation for boundary element method. *Engineering Analysis* 1999; **23**:257–265.
18. Menon G, Paulino GH, Mukherjee S. Analysis of hypersingular residuals error estimates in boundary element methods for potential problems. *Computer Methods in Applied Mechanics and Engineering* 1999; **173**: 449–473.
19. Muci-Küchler KH, Miranda-Valenzuela JC, Rudolphi TJ. Formulation of a new error indicator for adaptive meshing with Hermite boundary elements. *Computer Methods in Applied Mechanics and Engineering* 1999; **173**:419–431.
20. Muci-Küchler KH, Miranda-Valenzuela JC. A new error indicator based on stresses for adaptive meshing with Hermite boundary elements. *Engineering Analysis* 1999; **23**:657–670.
21. Miranda-Valenzuela JC, Muci-Küchler KH, Soriano-Soriano S. Adaptive meshing in thermoelasticity using Hermite boundary elements. In *Proceedings of the Boundary Elements Techniques Conference*, Aliabadi MH (ed.), London, 1999; 261–272.
22. Zienkiewicz OC, Zhu JZ. The superconvergent patch recovery and a posteriori error estimates. Part 1: the recovery technique. *International Journal for Numerical Methods in Engineering* 1992; **33**:1331–1364.
23. Zienkiewicz OC, Zhu JZ. The superconvergent patch recovery and a posteriori error estimates. Part 2: Error estimates and adaptivity. *International Journal for Numerical Methods in Engineering* 1992; **33**:1365–1382.
24. Tessler A, Riggs HR, Dambach M. A novel four-node quadrilateral smoothing element for stress enhancement and error estimation. *International Journal for Numerical Methods in Engineering* 1999; **44**:1527–1543.
25. Muci-Küchler KH, Rudolphi TJ. A weakly singular formulation of traction and tangent derivative boundary integral equations in three-dimensional elasticity. *Engineering Analysis* 1993; **11**:195–201.
26. Muci-Küchler KH, Rudolphi TJ. Application of tangent derivative boundary integral equations to the formulation of higher order boundary elements. *International Journal of Solids and Structures* 1994; **31**:1565–1584.
27. Muci-Küchler KH, Miranda-Valenzuela JC. A new error indicator based on stresses for three-dimensional elasticity. *Engineering Analysis*, Special issue on adaptive meshing and error estimation. 2001, in press.
28. Rencis JJ, Mullen RL. Solution of elasticity problems by a self-adaptive mesh refinement technique for boundary element computation. *International Journal for Numerical Methods in Engineering* 1986; **23**:1509–1527.
29. Rencis JJ, Mullen RL. A self adaptive mesh refinement technique, *Computational Mechanics* 1988; **3**:309–319.
30. Rodríguez JJ, Power H. A mesh refinement technique for the boundary element method based on local error analysis. In *Proceedings of the Boundary Elements XXI Conference*, Brebbia CA, Power H (eds). WIT Press: 1999; 291–302.
31. Timoshenko SP, Goodier JN. *Theory of Elasticity* (Third edn.). McGraw-Hill International, 1970.
32. M. Guiggiani, Error indicators for adaptive mesh refinement in the boundary element method—A new approach. *International Journal for Numerical Methods in Engineering* 1990; **29**:1247–1269.
33. Chao RM, Lee SY. An *h*-adaptive refinement BEM procedure using modified sample point error analysis in two-dimensional elastic problems. *Advances in Engineering Software* 1999; **30**:227–242.

